CeO_2Dopingof $Hf_{0.5}Zr_{0.5}O_2$ Thin Films for High Endurance Ferroelectric Memories

Zhouchangwan Yu, Balreen Saini, Pei-Jean Liao, Yu-Kai Chang, Duen-Huei Hou, Chih-Hung Nien, Yu-Cuan Shih, Sai Hooi Yeong, Valeri Afanas'ev, Fei Huang, John Baniecki, Apurva Mehta, Chih-ShengChang, H.-S. Philip Wong, Wilman Tsai, Paul McIntyre**

Z. Yu

Department of Electrical Engineering, Stanford University, Stanford, CA 94305, USA

E-mail: zyu21@stanford.edu

B. Saini

Department of Materials Science and Engineering, Stanford University, Stanford, CA 94305, USA

Dr. P.J. Liao, Dr. Y.K. Chang, Dr. D.H. Hou, Dr. C.H. Nien, Dr.Y.C. Shih, Dr. S.H. Yeong,

Taiwan Semiconductor Manufacturing Company, Hsinchu 300-091, Taiwan

Prof. Valeri Afanas'ev

Department of Physics and Astronomy, University of Leuven, 3001 Leuven, Belgium

F. Huang

Department of Electrical Engineering, Stanford University, Stanford, CA 94305, USA

Dr. J.D. Baniecki, Dr. A. Mehta

SLAC National Accelerator Laboratory, Menlo Park, CA 94025, USA

Dr. C.S. Chang

Taiwan Semiconductor Manufacturing Company, Hsinchu 300-091, Taiwan

Prof. H.-S.P. Wong,

Department of Electrical Engineering, Stanford University, Stanford, CA 94305, USA

Prof. W. Tsai

Department of Materials Science and Engineering, Stanford University, Stanford, CA 94305, USA

Prof. P.C. McIntyre
Department of Materials Science and Engineering, Stanford University, Stanford, CA 94305, USA
SLAC National Accelerator Laboratory, Menlo Park, CA 94025, USA
E-mail: pcm1@stanford.edu

Keywords: Ferroelectric memories, ferroelectric HZO, CeO_2

We demonstrate ferroelectric switching in CeO_2-doped $Hf_{0.5}Zr_{0.5}O_2$ (HZCO) thin films and their applications for back-end-of-line (BEOL) compatible embedded memories. At low cerium oxide doping concentrations (2.0 - 5.6 mol%), the ferroelectric orthorhombic phase is stabilized after annealing at temperatures below 400 ℃. HZCO ferroelectrics show reliable switching characteristics beyond 10^{11} cycles in TiN/HZCO/TiN (MFM) capacitors, several orders magnitude higher than the identically processed $Hf_{0.5}Zr_{0.5}O_2$ (HZO) capacitors, without sacrificing polarization and retention.Internal photoemission and photoconductivity experiments show that CeO_2-doping introduces in-gap states in HZCO that are nearly aligned with TiN Fermi level, facilitating the electron injection through these states. The enhanced background conductivity, which may lead to more uniform thermal dissipation in the HZCO films, delays the irreversible degradation that leads to the device failures.

1. Introduction

The observation of ferroelectricity inHfO_2-based metal oxide thin filmsoriginates from the formation of the metastable, non-centrosymmetric polar orthorhombic $Pca2_1$ (O) phase of HfO_2[1]. Since the discovery of ferroelectricity in doped HfO_2 in 2011[1], many dopants including Si[1], Al[2], Y[3], and La[4] have been studied to promote formation of the polar O-phase of HfO_2. In addition, ferroelectric binary alloys of HfO_2 and ZrO_2 (HZO) that exhibit a full range of solid solubility are of particular interest, as the O-phase can be stabilized over a wide range of composition[5]and forms from initially-amorphous as-deposited material after crystallization anneals performed at relatively low temperatures[6].

HZO based ferroelectric (FE) materials are promising for semiconductor memory applications such as 1T1C FE random-access-memories(FeRAMs) and nonvolatile FE field-effect-transistors (FeFETs) due to their ability to scale down to ultra-thin films and very small device dimensions, and their compatibility with silicon complementary metal oxide semiconductorback-end-of-line (BEOL) processing temperatures[7, 8]. Limited cycling endurance of the polarization is amajor challenge for implementation of HZO in commercial products developed for embedded memories. High endurance is essential for memory devices utilized in novel memory architectures designed forhigh throughput and energy efficiency, such as near-memory or in-memory computing architectures where memory is integrated with logic on the same chip [9]. For metal-ferroelectric-metal (MFM) capacitor structures, anti-ferroelectric (AFE) HZO[10] and FE La-doped HZO[11] have been demonstrated to enhance the endurance to 10^{10} – 10^{12} cycles. However, for FeFET structures where the ferroelectrics are inserted into the metal-ferroelectric-insulator-semiconductor (MFIS) gate stack, the cyclic endurance is further limited, as the SiO_2 or SiON interfacial layers can exhibit early failures during FE polarization switchingdue to the high electricfieldsdeveloped across these dielectric layers. Metal oxide-channel FeFETs[8] and back-gated FeFETs[12] are proposed to solve the problem by eliminating the interfacial layers, but direct implementation of top-gated FeFETs on siliconchannelsremains a key challenge.

Discovery of new compositions is one approachto improveferroelectric properties and reliability of HfO_2-based materials[11]. Doping HfO_2 with ceriumoxide (CeO_2), another fluorite-structure metal oxide,has been utilized to enhance the dielectric constant ofhigh-κ dielectrics [13-15]. CeO_2-HfO_2 films were crystallized after annealing at 900°C and were identified as tetragonal-(T) or cubic-(C) phase[13, 14]. Recently, ferroelectricity has also been demonstrated in CeO_2-doped HfO_2 due to the stabilization of the O-phase[16]. However, CeO_2 doping ofHZO solid solution to form HZCO ternary alloys and their reliability have not been explored. In HZCO solid solutions, non-ferroelectric tetragonal-(T) and monoclinic-(M) phases co-exist at high temperatures 1500°C across a fairly broad range of compositions[17]. The metastable ferroelectric O-phase, which is a structural distortion of the T-phase, may be promotedat low temperatures in HZCO thin films, as a result ofthe competition between the stable T- and M- phases.In addition to the ~6 eV energy gap between continuum states that is typically observed in transition metal oxides, CeO_2 also exhibit a smaller energy gap ~3.3 eV between the valence band and Ce 4f states[18, 19], which is typically considered as the band gap

of CeO_2[20-22]. The smaller band gap of CeO_2 compared to HfO_2 and ZrO_2, and the contribution of 4f electrons to its electronic structure, also provides opportunities for tuning the functional properties of HZCO alloys.

In this work, we report the first experimental investigation of ferroelectricity in HZCO thin films. High polarization and very reliable switching characteristics are achieved beyond 10^{11} cycles in MFM capacitors. High endurance ($>10^{10}$ cycles) is also demonstrated in MFIS gate stacks for FeFET applications. Polarization cycling characteristicsare systematically studied usingstress-induced leakage current (SILC) analysis, indicating thatCeO_2 doping delays irreversibledegradation of the FE layers that is a precursor of dielectric breakdown. Mechanisms responsible for the observed CeO_2 doping effects are probed using photoconductivity (PC) and internal photoemission (IPE) measurements, indicating the importance of electronic conduction through in-gap states contributed by Ce ion doping of the HZCO. Considering the bulk electronic structure of CeO_2, these states are likely predominantly 4f in character.

2. Results and Discussions

2.1. Material Characterizations

A scanning transmission electron microscopy (STEM) image of a 3.8% CeO_2 HZCO MFM structure in **Figure 1a** clearly shows crystalline grains across the film thickness, indicating

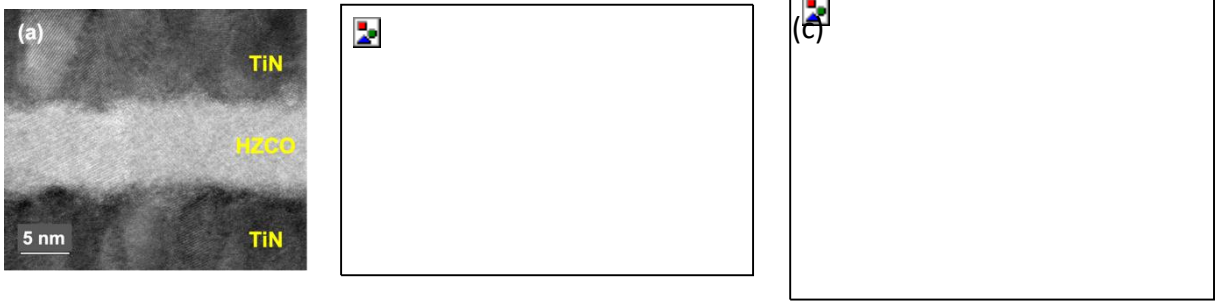

full crystallization of HZCO films after RTA at 400 ℃. Elemental mapping using energy dispersive X-ray spectroscopy (EDS) reveals uniform detection of Hf, Zr, and Ce across the film without evidence of local CeO_2 segregation, as shown in **Figure 1b**. **Figure 1c** depicts the grazing incidence X-ray diffraction (Gi-XRD) of HZO and HZCO films crystallized at 400 ℃. All films show a main peak around Q = 2.13 $Å^{-1}$, which matches the (111) orthorhombic peak[23]. The dominant O-phase is consistent with the observation offerroelectric polarization switching shown in later sections, for the investigated range of CeO_2 doping (2.0% - 5.6%).

Figure 1: (a) Scanning transmission electron microscopy - low-angle annular dark field (STEM-LAADF) image and (b) EDS elemental mappings of TiN/HZCO/TiN stack, indicating CeO_2 is uniformly doped across HZO without segregation. (c) Gi-XRD of HZO and HZCO 9 nm films after RTA at 400 ℃, consistent with a dominant O-phase which is responsible for observed ferroelectricity.

2.2.HZCO MFM Characteristics

2.2.1. Polarization and Memory Characteristics

Figure 2a depicts the polarization-voltage (P-V) hysteresis curves of TiN/HZCO 9 nm/TiN capacitors synthesized by RTA at 400 ℃. CeO_2 doping modulates the polarization, showing a decreasing trend of polarization as CeO_2 concentration increases from 0 to 5.6%. HZCO capacitors exhibiteda polarizationretention $>10^4$ seconds at 85 ℃, as depicted in **Figure 2b**, where only <8% of the initial polarization was lost by the end of the measurement for all doping concentrations. A significant improvement of endurance as a result CeO_2 doping of otherwise identically processed HZO films is shown in **Figure 2c**. Identically processed HZO capacitors fail after 2×10^8 polarizationswitching cycles due to hard dielectric breakdown.

With CeO_2 doping, the maximum number of switching cycles increases with increasing doping concentration over the range of compositions studied. The 3.8% and 5.6% HZCO capacitors are switchable beyond 10^{11} cycles without breakdown, i.e., three orders of magnitude higher than HZO. All the HZO and HZCO capacitors exhibit a gradual increase of polarization at the beginning stage of the field cycling, followed by a gradual decrease of the polarization after a certain number of cycles, commonly called "wake-up" and "fatigue", respectively. With slight "wake-up" and "fatigue", the HZCO 3.8% capacitors maintain polarization higher than 17 $\mu C/cm^2$ throughout cycling, as shown in **Figure 2c**.

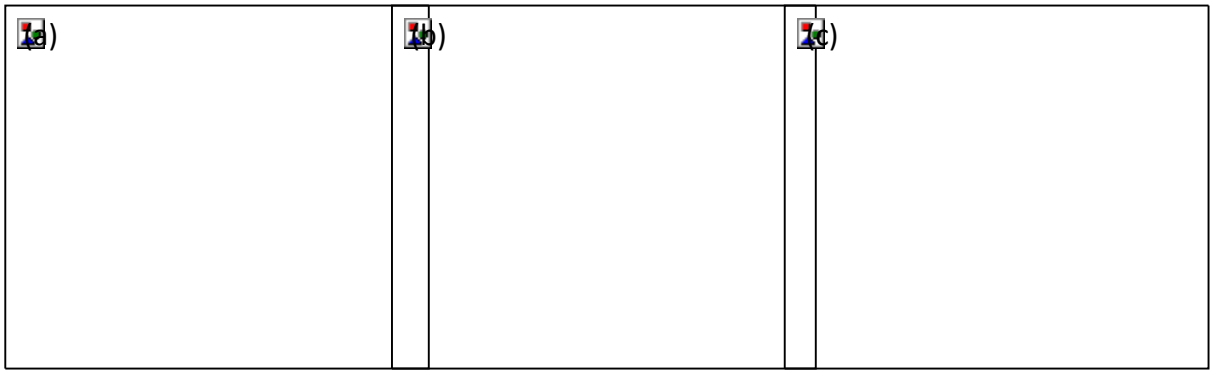

Figure 2: (a) P-V hysteresis after 10^5 wake-up cycles, (b) retention at 85 ℃, and (c) endurance of TiN/HZCO/TiN capacitors with various CeO_2 doping. The stacks were annealed post deposition at 400 ℃ for 30s. The HZCO 3.8% capacitor switched using ± 3 V 100 ns pulses still functionsafter 10^{11} cycles with P_{sw}> 17μC/cm^2.

2.2.2 Leakage Current and Conduction Mechanism in HZCO

In contrast to the suggestion that high switching endurance may be correlated with low defect density, and thus to low leakage current[24], the HZCO capacitors generally exhibit greater electronic conductionthan the identically processed HZO devices, as shown in **Figure 3a**. Interestingly, the breakdown voltage (V_{BD}) is greatly increased by CeO_2 doping (**Figure 3b**). The bias asymmetry of the positive and negative current densitiesand V_{BD} is due to the asymmetry of the top and bottom TiN electrodes. Although the deposition method of the top and bottom TiN is the same, the bottom TiN is oxidized under oxygen plasma exposure during PE-ALD (see O elemental mapping in **Figure 1b**), producing a TiO_x–containing layer at the bottom interface. A higher conductivity and V_{BD} of the films may be correlated with the better endurance properties.

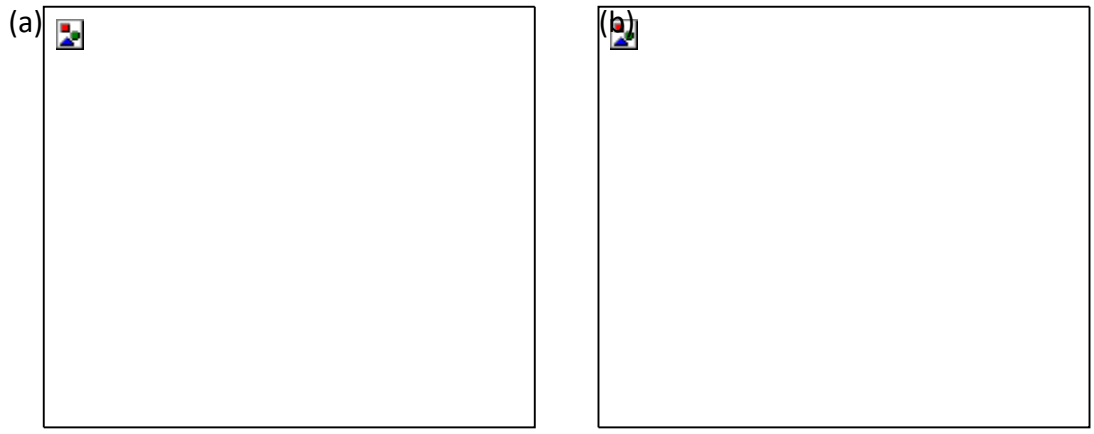

Figure 3: (a) Leakage current of HZCO capacitors before cycling, indicating higher leakage conduction induced by CeO_2 doping. Before I-V measurements, a pre-poling was applied on the device by ±3 V bias. (b) Breakdown voltages of HZCO 9 nm films. CeO_2 doping greatly increases the breakdown voltage of HZO films.

Enhanced electronic conduction associated with CeO_2 doping may be explained by incorporation of Ce-related in-gap states enabling electron injection into the ferroelectric layer that is less damaging to the "host" HZO matrix[22]. Indeed, the results of PC measurements illustrated in **Figure 4a** and **Figure 4b** indicate that while both HZO and HZCO exhibit an energy gap of 5.5 eV, the CeO_2-doping results in appearance of an additional PC threshold at 3.5 eV indicating Ce-related states in the HZO gap. In bulk CeO_2, the lowest unoccupied states stem from the localized atomic-like Ce 4f states, energetically positioned 3 eV above the O-2p derived valence band (VB) top[18, 19]. If the additional PC threshold at 3.5 eV results from optically excited electronic transitions from the VB top to these empty Ce 4f in-gap states within the 5.5-eV wide HZO band gap; Therefore these states appear to be ≈ 2 eV below the HZO conduction band (CB) minimum. This energy position is nearly aligned with the Fermi level of the TiN electrode, as indicated by the corresponding 2.2eV electron photoemission threshold from TiN into undoped HZO film **Figure 4a**. This would facilitate selective electron injection into these Ce-derived states as illustrated in **Figure 4c**, possibly suppressing injection-induced degradation of the HZO matrix by preventing electron injection into the Hf- and Zr-derived CB states. The alternative possibility that the PC threshold at 3.5 eV originates from electron transition from some in-gap states to the CB minimum, placing the hypothetical occupied states 3.5 eV below the CB minimum is unlikely since CeO_2

insulators deposited on semiconductors, e.g. Ge [see ref. below] exhibit low interface trap density despite considerable leakage currents indicative of low CB offset [20].

Ref:

Brunco, DP (Brunco, D. P.) Dimoulas, A (Dimoulas, A.) Boukos, N (Boukos, N.) Houssa, M (Houssa, M.) Conard, T (Conard, T.) Martens, K (Martens, K.) Zhao, C (Zhao, C.) Bellenger, F (Bellenger, F.) Caymax, M (Caymax, M.) Meuris, M (Meuris, M.) Heyns, MM (Heyns, M. M.), J. Appl. Phys. 2007 vol. 102 (2) 024104.

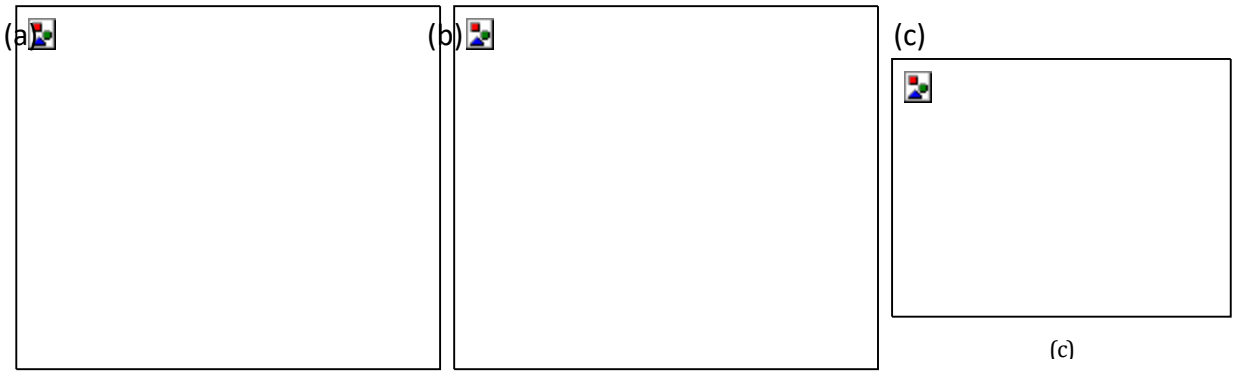

Figure 4: Photocurrent quantum yield plots in $Y^{1/2} - h\nu$coordinates illustrating determination of the spectral thresholds for 10 nm Au/9 nm HZO/10 nm TiN (a) and Au/9 nm HZCO/10 nm TiN (b) structures, where Au is deposited after post-metal RTA and top TiN removal by wet etch. Vertical arrows indicate the inferred spectral thresholds of electron photoemission from TiN into HZO and the PC onsets corresponding to the bandgap of HZO (in the inset) and CeO_2.(c) Schematic diagram of PC and IPE processes at HZCO/TiN BE interface, showing that the Ce-related in-gap states are nearly aligned with the TiN Fermi level.

One concern related to leakage conduction in ferroelectrics is that mobile charges in the bulk of the ferroelectric layer can internally screen the polarization and thus give poor retention characteristics. However, the retention of the capacitors is not sacrificedas a result of CeO_2 doping, as shown in **Figure 2b**. All the HZCO capacitors exhibited polarization retention greater than10^4 seconds at 85 °C with very minor polarization loss at the end of the measurements. In addition, for applications in ferroelectric non-volatile memories, the devices are normally not under bias. Therefore, higher steady state leakage currents in HZCO compared to HZO should not contribute significantly to power dissipation or loss of the memory window as a function of time.

2.2.3. Stress-Induced Leakage Current (SILC)

To understand the observed effect of CeO_2 doping on bipolar voltage cycling behavior, SILC is monitored to characterize the leakage evolution with a 0.4 V/sec ramp rate DC I-V measurement (**Figure 5**). The occurrence of polarization fatigue and dielectric breakdown in HZO samples is accompanied by an increase in SILC (**Figure 6**), where the steep degradation detected after 10^5 cycles (i.e. 2× SILC increase) maybe associated with a thermal runaway phenomena[25]. HZCO MFM capacitors exhibited 10× better endurance based on a 2× SILC criteria and more than 1000× better endurance before dielectric breakdown occurs. In addition, the rate of SILC increase is also suppressed by increasing the CeO_2 doping.
This suggests the prevention of localized heating, which may result from the higher conductivity of HZCO being caused by different transport mechanisms, such as polaron hopping in Ce in-gap states[26]. Localized enhancement of electronic conduction in semiconducting and insulating metal oxides mediated by locally-varying defect populations is common and can lead to localized breakdown events, which can be either hard[27-29] or soft, as in RRAM filament formation[30]. Increasing the average bulk conductivity by CeO_2 doping will tend to reduce the impact of such local sources of incipient breakdown events by reducing the current carried along these paths.

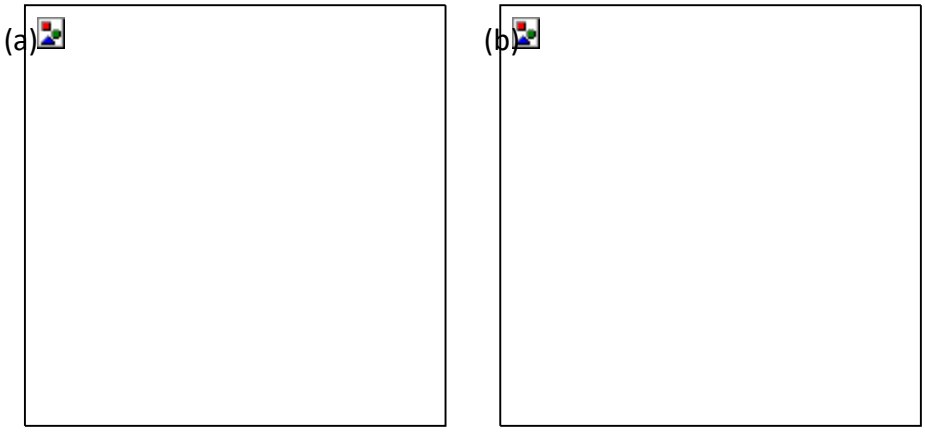

Figure 5: SILC spectrum upon ± 3V 500 ns endurance in HZO (a) and 3.8% HZCO (b). Obvious SILC phenomenon is shown in HZO before 5×10^7-cycle, leading to dielectric hard

breakdown. The reduced contributionof HK shallow traps tothe HZCO SILC spectrum coincides with less than 10× SILC increase after10^8polarization switching cycles.

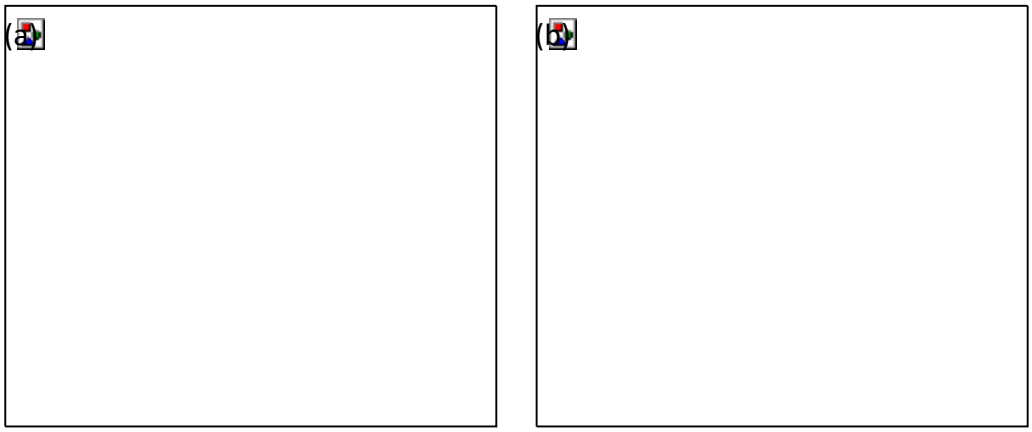

Figure 6: SILC as a function of cycle number in (a) HZO and (b) HZCO capacitors under ±3V 500ns switching. HZCO exhibited a 10× improvement in endurance based on a 2× SILC criterionand a smallerSILC degradation rate forincreasing CeO_2mol%. The apparent suppression of local thermal runaway provides > 10^{10}-cycle endurance forHZCO.

2.2.4. Low Temperature Crystallizationof O-HZCO

Low crystallization temperatures enable a broader range of applications of ferroelectrics in on-chip electronics. For example, novel back-end-of-line compatible nonvolatile memory devices such as metal oxide-channel FeFETs require low processing temperatures to prevent the channel oxide degradation. The RTA temperature to stabilize the O-phase HZCO can be further reduced to 350 ℃ by increasing the RTA time. **Figure 7a** and **Figure 7b** depict the PV hysteresis and Gi-XRD showing phase evolution of 350℃ annealed HZCO capacitors as a function of RTA time. High polarization (>40$\mu C/cm^2$) is achieved after an RTA ofonly 300 second duration at 350 ℃. The (111)orthorhombic peak intensity increases ~ 9 times from 30 seconds to 300 seconds, indicating greater crystallinity as the annealing time increases, consistent with the increasing trend of polarization.

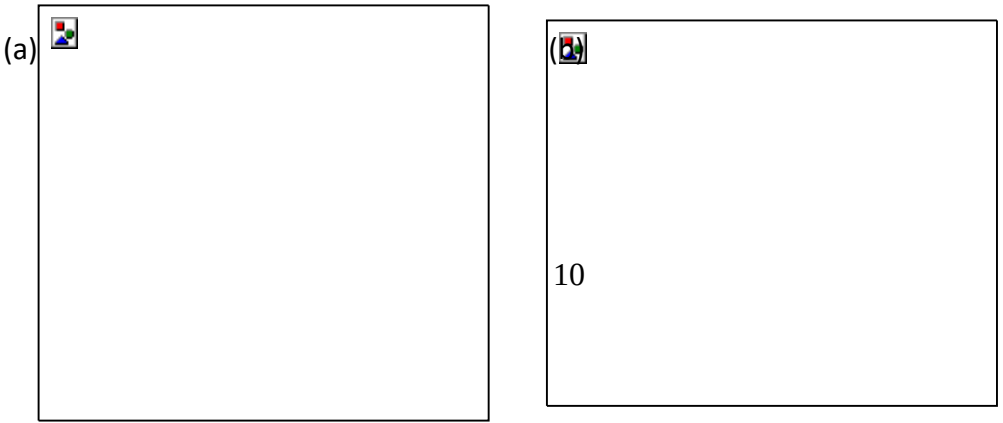

Figure 7: (a) P-V hysteresis and (b) GI-XRD of HZCO 3.8% capacitors annealed at 350 ℃ for various duration. The (111)orthorhombic peak intensity increases about 9 times from 30 seconds to 300 seconds,indicating higher crystallinity as the annealing time increases.

2.3.HZCO MFIS Switching Endurance

Among the various on-chip ferroelectric memory structures, FeFETsare of great interest due to their non-destructive read operation and simple, highly-scalable cell structure (1T)[9, 31]. HfO_2-based ferroelectric materials in metal-ferroelectric-insulator-semiconductor (MFIS) gate stacks often have unnecessarily high polarization[32, 33], setting up ahigh electric field across the interfacial insulator layer during polarization switching, and thus leading to early device failure[34-36]. Müller *et al*[32] reported from simulations that a spontaneous polarization between 5 – 10 μC/cm^{2}is optimized for maintaining a memory window > 1 V while keeping low electric field across the interfacial layers. Therefore, we utilized HZCO films of 7 nm thickness inserted inMFIS gate stacks to satisfy the condition forsufficient, but not excessive,polarization for threshold voltage switching of a FeFET device[32, 33]. **Figure 8a** is a representative cross-sectionalTEM image ofa HZCO 3.8% MFIS stack. The HZCO thin film deposited on a Si (100) substrate, with a SiO_2 interfacial layer of 1.7 nm thickness present after RTA. The pristine state polarization of the 7 nm HZCO 3.8% MFIS gate stack is less than that of an otherwise identicalHZO stack, but it endures 10^{10} switching cycles before breakdown, 10^5× higher than the similarlyprocessed and tested HZO MFIS, as shown in **Figure 8b**. The HZCO MFIS gate stack displays a slight polarization "wake-up" followed by "fatigue", but the switching polarization remains less than $10\mu C/cm^2$ throughout endurance testing. This is preferred for MFIS gate stacks to alleviate the high polarization bound charge density at the semiconductor channel and the high electric field across the SiO_xinterlayer[32, 33]. The steady state leakage current follows a trend similar to the MFM structures, where the HZCO stack exhibits higher conductance than the HZO stack during the early stages of polarization switching. The sudden increase in current observed for HZO gate stacks isdelayed from 10^4 to 10^6 switching cycles,and the rate of current increase is greatly suppressed in HZCO, as shown in**Figure 8b**. The lower polarization and higher bulk conductivity of HZCO together may lead to a delay of hard breakdown compared to HZO, and hence shows promise for FeFET applications.

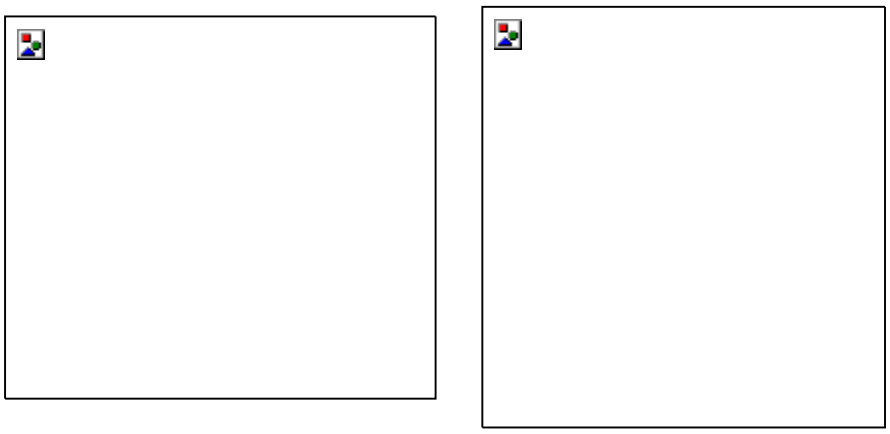

Figure 8: (a) STEM-LAADF image of TiN/HZCO/SiO_x/Si gate stack. The interlayer $SiO_x$is ~1.7 nm. (b) Endurance and (c) SILC of MFIS stacks with 7 nm HZO and HZCO 3.8%, annealed post deposition at 600℃ for 30s and cycled by ±4 V 500 ns pulses. The HZCO 3.8% MFIS capacitor displays endurance $>10^{10}$ cycles with preferred low polarization.

3. Conclusion

In this work, we demonstrate ferroelectric switching in CeO_2-doped HZO with high endurance and high retention. CeO_2-doping introduces extra in-gap states in HZCO that are closelyaligned with the TiN Fermi level, facilitating electron injection through these states, and thus suppressing injection-induced damages in the ferroelectric layers. Although the leakage currents in HZCO arehigher than thosein HZO under identical experimental conditions prior to polarization cycling, the stress-induced-leakage-current increase due to cycling degradation is delayed, and the rate of current increase is also suppressed compared to HZO, enabling reliable operation beyond 10^{11} cycles of polarization switching. By applying HZCO with reduced thickness and low but sufficient polarization in the MFIS structures, high endurance beyond 10^{10} cycles can be achieved, showing a promising route to reliable FeFET operation.

4. Experimental Section

Device Fabrication:

TiN/HZCO/TiN (MFM) capacitors: The HZCO thin films were deposited by plasma enhanced – atomic layer deposition (PE-ALD) with intermittent pulses of Hf, Zr, and Ce precursors and oxygen plasma as the co-reactant. Each ALD super cycle contained one HfO_2, one ZrO_2, and "n" CeO_2 cycles, where the Ce content was controlled by varying the number of CeO_2 cycles. The HZCO thin film was sandwiched between TiN top and bottom electrodes deposited by sputtering. A post-metal rapid thermal anneal (RTA) is performed at 350 - 400 ℃ to crystallize the HZCO. For electrical measurements, Pt top contacts were deposited by e-beam evaporation and patterned by photolithography. Top TiN was then selectively wet etched by SC1 solution with Pt pads as masks.

TiN/HZCO/SiO_x/p+ Si (MFM) capacitors: p+ Si wafers were cleaned by RCA process (SC1-SC2-HF). Immediately after, HZCO 7 nm were deposited on Si, followed by TiN 10 nm deposition by sputtering. A post-metal rapid thermal anneal (RTA) is performed at 600 ℃ to crystallize the HZCO. The process to pattern the metal contacts was the same as that of the MFM capacitors.

Characterizations:
The electrical measurements in this work are performed using HP 4156C and Keithley 4200-SCS Parameter Analyzers. The polarization during field cycling was read by positive-up-negative-down (PUND) measurements with the same waveform as the cycling pulses.The Gi-XRD measurements were performed at beamline 2-1 of the Stanford Synchrotron Radiation Lightsource (SSRL), SLAC National Accelerator Laboratory.

Acknowledgements
This work is supported by the Semiconductor Research Corporation through nCORE Task 2966.009 of the IMPACT Center and by Stanford Non-volatile Memory Technology Research Initiative (NMTRI).Part of this work was performed at the Stanford Nanofabrication Facility (SNF) and Stanford Nano Shared Facilities (SNSF), supported by the National Science Foundation under award ECCS-2026822. Use of the SSRL, SLAC National Accelerator Laboratory, is supported by the U.S. Department of Energy (DEAC02-76SF00515). We acknowledge valuable discussions with Prof. A. Kummel (UCSD), Prof. K. Cho and Dr. K. Chae (UT Dallas), Prof. Y. Nishi (Stanford), Dr. M. Moinpour (EMD Electronics), and Dr. Y.-M. Lin (TSMC).

Received: ((will be filled in by the editorial staff))
Revised: ((will be filled in by the editorial staff))
Published online: ((will be filled in by the editorial staff))

((**For Reviews and Perspectives,**please insert author biographies and photographs herefor those authors who should be highlighted, max. 100 words each))

Author Photograph(s) ((40 mm broad, 50 mm high, color or grayscale))

The table of contents entry should be 50–60 words long and should be written in the present tense. The text should be different from the abstract text.

Z. Yu*, B. Saini, P.J. Liao, Y.K. Chang, D.H. Hou, C.H. Nien, Y.C. Shih, S.H. Yeong, V. Afanas'ev, F. Huang, J.D. Baniecki, A. Mehta, C.S. Chang, H.-S.P. Wong, W. Tsai, P.C. McIntyre*

CeO_2-Doped $Hf_{0.5}Zr_{0.5}O_2$ Ferroelectrics for High Endurance Embedded Memory Applications

In this work, enhanced cycling endurance is demonstrated in ferroelectric CeO_2 doped $Hf_{0.5}Zr_{0.5}O_2$ (HZCO) thin films. CeO_2 doping places extra in-gap states in the HZCO bandgap that are nearly aligned to the TiN electrodes, facilitating selective electron injections less damaging to the host HZO matrix, and suppressing the film degradation cause by thermal runaway.

ToC figure ((Please choose one size: 55 mm broad × 50 mm high **or** 110 mm broad × 20 mm high. Please do not use any other dimensions))

((Supporting Information can be included here using this template))

Supporting Information

Title ((no stars))

*Author(s), and Corresponding Author(s)** ((write out full first and last names))

((Please insert your Supporting Information text/figures here. Please note: Supporting Display items, should be referred to as Figure S1, Equation S2, etc., in the main text…)

References

[1] T. S. Böscke, J. Müller, D. Bräuhaus, U. Schröder, U. Böttger, *Applied Physics Letters***2011**, *99*, 102903.

[2] S. Mueller, J. Mueller, A. Singh, S. Riedel, J. Sundqvist, U. Schroeder, T. Mikolajick, *Advanced Functional Materials***2012**, *22*, 2412.

[3] J. Müller, U. Schröder, T. S. Böscke, I. Müller, U. Böttger, L. Wilde, J. Sundqvist, M. Lemberger, P. Kücher, T. Mikolajick, L. Frey, *Journal of Applied Physics***2011**, *110*, 114113.

[4] U. Schroeder, C. Richter, M. H. Park, T. Schenk, M. Pešić, M. Hoffmann, F. P. G. Fengler, D. Pohl, B. Rellinghaus, C. Zhou, C.-C. Chung, J. L. Jones, T. Mikolajick, *Inorganic Chemistry***2018**, *57*, 2752.

[5] J. Müller, T. S. Böscke, U. Schröder, S. Mueller, D. Bräuhaus, U. Böttger, L. Frey, T. Mikolajick, *Nano Letters***2012**, *12*, 4318.

[6] J. Müller, T. S. Böscke, D. Bräuhaus, U. Schröder, U. Böttger, J. Sundqvist, P. Kücher, T. Mikolajick, L. Frey, *Applied Physics Letters***2011**, *99*, 112901.

[7] T. Francois, L. Grenouillet, J. Coignus, P. Blaise, C. Carabasse, N. Vaxelaire, T. Magis, F. Aussenac, V. Loup, C. Pellissier, S. Slesazeck, V. Havel, C. Richter, A. Makosiej, B. Giraud, E. T. Breyer, M. Materano, P. Chiquet, M. Bocquet, E. Nowak, U. Schroeder, F. Gaillard, In *2019 IEEE International Electron Devices Meeting (IEDM)*, 7-11 Dec. 2019, **2019**.

[8] S. Dutta, H. Ye, W. Chakraborty, Y. C. Luo, M. S. Jose, B. Grisafe, A. Khanna, I. Lightcap, S. Shinde, S. Yu, S. Datta, In *2020 IEEE International Electron Devices Meeting (IEDM)*, 12-18 Dec. 2020, **2020**.

[9] A. I. Khan, A. Keshavarzi, S. Datta, *Nature Electronics***2020**, *3*, 588.

[10] S. C. Chang, N. Haratipour, S. Shivaraman, T. L. Brown-Heft, J. Peck, C. C. Lin, I. C. Tung, D. R. Merrill, H. Liu, C. Y. Lin, F. Hamzaoglu, M. V. Metz, I. A. Young, J. Kavalieros, U. E. Avci, In *2020 IEEE International Electron Devices Meeting (IEDM)*, 12-18 Dec. 2020, **2020**.

[11] A. G. Chernikova, M. G. Kozodaev, D. V. Negrov, E. V. Korostylev, M. H. Park, U. Schroeder, C. S. Hwang, A. M. Markeev, *ACS Applied Materials & Interfaces***2018**, *10*, 2701.

[12] A. A. Sharma, B. Doyle, H. J. Yoo, I. C. Tung, J. Kavalieros, M. V. Metz, M. Reshotko, P. Majhi, T. Brown-Heft, Y. J. Chen, V. H. Le, In *2020 IEEE International Electron Devices Meeting (IEDM)*, 12-18 Dec. 2020, **2020**.

[13] P. R. Chalker, M. Werner, S. Romani, R. J. Potter, K. Black, H. C. Aspinall, A. C. Jones, C. Z. Zhao, S. Taylor, P. N. Heys, *Applied Physics Letters***2008**, *93*, 182911.

[14] W.-H. Kim, M.-K. Kim, I.-K. Oh, W. J. Maeng, T. Cheon, S.-H. Kim, A. Noori, D. Thompson, S. Chu, H. Kim, *Journal of the American Ceramic Society***2014**, *97*, 1164.

[15] W. J. Maeng, I.-K. Oh, W.-H. Kim, M.-K. Kim, C.-W. Lee, C. Lansalot-Matras, D. Thompson, S. Chu, H. Kim, *Applied Surface Science***2014**, *321*, 214.

[16] T. Shiraishi, S. Choi, T. Kiguchi, T. Shimizu, H. Funakubo, T. J. Konno, *Applied Physics Letters***2019**, *114*, 232902.

[17] E. R. Andrievskaya, G. I. Gerasimyuk, O. A. Kornienko, A. V. Samelyuk, L. M. Lopato, V. P. Red'ko, *Powder Metallurgy and Metal Ceramics***2006**, *45*, 448.

[18] E. Wuilloud, B. Delley, W. D. Schneider, Y. Baer, *Physical Review Letters***1984**, *53*, 202.

[19] N. V. Skorodumova, R. Ahuja, S. I. Simak, I. A. Abrikosov, B. Johansson, B. I. Lundqvist, *Physical Review B***2001**, *64*, 115108.

[20] V. V. Afanas'ev, S. Shamuilia, A. Stesmans, A. Dimoulas, Y. Panayiotatos, A. Sotiropoulos, M. Houssa, D. P. Brunco, *Applied Physics Letters***2006**, *88*, 132111.

[21] V. V. Afanas'ev, A. Stesmans, *Journal of Applied Physics***2007**, *102*, 081301.

[22] S. Shamuilia, V. V. Afanas'ev, A. Stesmans, I. McCarthy, S. A. Campbell, M. Boutchich, M. Roeckerath, T. Heeg, J. M. J. Lopes, J. Schubert, *Journal of Applied Physics***2008**, *104*, 114103.

[23] M. H. Park, H. J. Kim, Y. J. Kim, W. Lee, T. Moon, C. S. Hwang, *Applied Physics Letters***2013**, *102*, 242905.

[24] M. Pešić, F. P. G. Fengler, L. Larcher, A. Padovani, T. Schenk, E. D. Grimley, X. Sang, J. M. LeBeau, S. Slesazeck, U. Schroeder, T. Mikolajick, *Advanced Functional Materials***2016**, *26*, 4601.

[25] S. W. Chang, K. Joshi, P. J. Liao, J. R. Shih, Y. Lee, In *2017 IEEE International Reliability Physics Symposium (IRPS)*, 2-6 April 2017, **2017**.

[26] H. L. Tuller, A. S. Nowick, *Journal of Physics and Chemistry of Solids***1977**, *38*, 859.

[27] K. F. Schuegraf, C. Hu, *Semiconductor Science and Technology***1994**, *9*, 989.

[28] S. Lombardo, J. H. Stathis, B. P. Linder, K. L. Pey, F. Palumbo, C. H. Tung, *Journal of Applied Physics***2005**, *98*, 121301.

[29] L. Vandelli, A. Padovani, L. Larcher, G. Bersuker, *IEEE Transactions on Electron Devices***2013**, *60*, 1754.

[30] H. P. Wong, H. Lee, S. Yu, Y. Chen, Y. Wu, P. Chen, B. Lee, F. T. Chen, M. Tsai, *Proceedings of the IEEE***2012**, *100*, 1951.

[31] T. Mikolajick, U. Schroeder, S. Slesazeck, *IEEE Transactions on Electron Devices***2020**, *67*, 1434.

[32] J. Muller, P. Polakowski, S. Muller, H. Mulaosmanovic, J. Ocker, T. Mikolajick, S. Slesazeck, S. Muller, J. Ocker, T. Mikolajick, S. Flachowsky, M. Trentzsch, In *2016 16th Non-Volatile Memory Technology Symposium (NVMTS)*, 17-19 Oct. 2016, **2016**.

[33] S. Deng, Z. Liu, X. Li, T. P. Ma, K. Ni, *IEEE Electron Device Letters***2020**, *41*, 1348.

[34] E. Yurchuk, S. Mueller, D. Martin, S. Slesazeck, U. Schroeder, T. Mikolajick, J. Müller, J. Paul, R. Hoffmann, J. Sundqvist, T. Schlösser, R. Boschke, R. v. Bentum, M. Trentzsch, In *2014 IEEE International Reliability Physics Symposium*, 1-5 June 2014, **2014**.

[35] K. Ni, P. Sharma, J. Zhang, M. Jerry, J. A. Smith, K. Tapily, R. Clark, S. Mahapatra, S. Datta, *IEEE Transactions on Electron Devices***2018**, *65*, 2461.

[36] N. Gong, T. Ma, *IEEE Electron Device Letters***2018**, *39*, 15.

((References should be superscripted and appear after punctuation.[1,2] If you have used reference management software such as EndNote to prepare your manuscript, please convert the fields to plain text by selecting all text with [ctrl]+[A], then [ctrl]+[shift]+[F9]).[3–5] Footnotes should not be used in the text. Instead, additional information can be added to the Reference list. Please define all acronyms except IR, UV, NMR, and DNA or similar (for a list of acronyms not requiring definition, please see the list available on the journal homepage in our "Author Guidelines" section.))